The role of declining Arctic sea ice in recent decreasing terrestrial Arctic snow depths

Hotaek Park[*1], John E. Walsh[2], Yongwon Kim[2], Taro Nakai[2], and Tetsuo Ohata[1]

1 Research Institute for Global Change, JAMSTEC, Yokosuka, 237-0061, Japan
2 International Arctic Research Center, University of Alaska Fairbanks, Fairbanks, AK 99775, USA

* Corresponding Author
e-mail: park@jamstec.go.jp

Abstract

The dramatic decline in Arctic sea ice cover is anticipated to influence atmospheric temperatures and circulation patterns. These changes will affect the terrestrial climate beyond the boundary of the Arctic, consequently modulating terrestrial snow cover. Therefore, an improved understanding of the relationship between Arctic sea ice and snow depth over the terrestrial Arctic is warranted. We examined responses of snow depth to the declining Arctic sea ice extent in September, during the period of 1979–2006. The major reason for a focus on snow depth, rather than snow cover, is because its variability has a climatic memory that impacts hydrothermal processes during the following summer season. Analyses of combined data sets of satellite measurements of sea ice extent and snow depth, simulated by a land surface model (CHANGE), suggested that an anomalously larger snow depth over northeastern Siberia during autumn and winter was significantly correlated to the declining September Arctic sea ice extent, which has resulted in cooling temperatures, along with an increase in precipitation. Meanwhile, the reduction of Arctic sea ice has amplified warming temperatures in North America, which has readily offset the input of precipitation to snow cover, consequently further decreasing snow depth. However, a part of the Canadian Arctic recorded an increase in snow depth driven locally by the diminishing September Arctic sea ice extent. Decreasing snow depth at the hemispheric scale, outside the northernmost regions (i.e., northeastern Siberia and Canadian Arctic), indicated that Arctic amplification related to the diminishing Arctic sea ice has already impacted the terrestrial Arctic snow depth. The

strong reduction in Arctic sea ice anticipated in the future also suggests a potential long-range impact on Arctic snow cover. Moreover, the snow depth during the early snow season tends to contribute to the warming of soil temperatures in the following summer, at least in the northernmost regions.

Key words: sea ice extent, snow depth, land surface model, Arctic amplification, climatic memory

1. Introduction

The Arctic is warming faster than other regions of the Earth. The extent of the warming is exceeding values predicted by climate models (IPCC, 2008). A number of significant changes related to the warming have been found in climatic, ecological, and hydrological systems over the Arctic terrestrial region during the past few decades (Sturm et al., 2001; Serreze et al., 2000; Peterson et al., 2002). Most climate models also project that warming will continue, and thus the risks associated with these changes will further increase in the future.

Using *in situ* observations for 1875–2008, Bekryaev et al. (2010) found that air temperatures over the northern polar area have recorded the largest increase during the winter season. The warming winter temperature could affect the processes of snow accumulation and ablation over the Arctic. Recent studies have indicated a significant decrease in the snow-covered area over the Arctic during winter, in response to the increasing air temperature (Brown, 2000; McCabe and Wolock, 2010). The decrease in snow depth (SND) during the past few decades had also been identified by observation (Dyer and Mote, 2006) and simulation (Park et al., 2011b). In contrast, long-term *in situ* observations in northern Eurasia identified increasing SND trends (Bulygina et al., 2009; Kitaev et al., 2005). However, earlier occurrence of Arctic snowmelt and a substantial retreat of snow cover have been found during spring, based on satellite image analyses (Brown et al., 2010; Shi et al., 2011). The retreat of snow cover during spring is likely to contribute to increases in air temperature through positive radiative feedbacks (Groisman et al., 1994).

Snow impacts regional radiative and energy budgets, atmospheric circulation, and soil hydrothermal conditions (Groisman et al., 1994). Changes in SND therefore have climatic and hydrologic implications. Moreover, SND is a useful indicator of climate changes. The decrease in winter SND may not be influenced by just the increased winter temperature.

The winter SND depends largely on the conditions during the early snow season when snow starts to accumulate. Arctic warming has also resulted in later snow accumulation in autumn (Park et al., 2011b; Ye, 2001). Screen and Simmonds (2010) found that the warming in autumn is closely related to the retreat of Arctic sea ice. Of particular interest is the 40% reduction of sea ice extent (SIE) in summer 2007 compared to the local climatology (Comiso et al., 2008). This retreat is faster than the sea ice loss projected by climate models (IPCC, 2008), and it is assumed that the influence of the reduced autumn sea ice could accelerate winter Arctic warming. In reality, the decrease in the area of autumn Arctic sea ice is linked to changes in the Northern Hemisphere atmospheric circulation during winter (Cohen et al., 2012; Liu et al., 2011). Francis et al. (2009) documented that the atmosphere 'remembers' a reduction in summer sea ice cover, causing warming and destabilization of the lower troposphere in the following autumn and winter. These atmospheric changes will in turn affect the terrestrial climate and hydrology as a result of the atmosphere-land coupling. Ghatak et al. (2010) found that the increasing snow cover over Siberia during autumn and early winter was correlated with the decreasing September Arctic sea ice over the Pacific sector.

Snow cover influences energy and radiation budgets over the land surface through albedo feedback during periods when snow is present. SND has an important hydrological effect of enhancing soil moisture, which persists into the following summer, contributing to evaporation and river discharge. Furthermore, the history of snow evolution greatly influences the soil temperature in the following year through the insulation effect. That is, SND-hydrothermal effects appear after snowmelt. Considering the atmosphere-ocean-land coupling in the Arctic system, the effect of sea ice on SND is likely to persist through to the following summer. Therefore, it is necessary to investigate the relationship between SND in the early snow season and the preceding summer's sea ice. Understanding this relationship

51 may be important to projecting soil temperature and moisture in the following summer.
52 Climate models have projected a rapid decline of sea ice in the future (IPCC, 2008). The
53 projections suggest future changes in Arctic snow and therefore in hydrological processes in
54 the following summer.

55 The main objective of this study was to explore how the decline in Arctic
56 September sea ice extent (SIE) is linked to anomalously large SND variations over the Arctic
57 terrestrial region during 1979–2006. We focused on SND during the autumn and winter
58 seasons, which represent the snow accumulation period, and on September sea ice, which is
59 the month with a climatological minimum of sea ice cover. Therefore, observed variations in
60 SND could include any signals of changes emerging in the link between snowpack and
61 decreasing SIE. The reason why we focused on SND, rather than snow cover, is because the
62 influence of SND can persist through to the following summer as the aforementioned climate
63 memory. Most of the previous studies that have examined the relationship between changing
64 sea ice cover and snow have focused on snow cover, linked to changes in the Northern
65 Hemisphere atmospheric climate in the winter (Francis et al., 2009; Liu et al., 2012; Cohen et
66 al., 2012). Park et al. (2011b) described the spatiotemporal trends and variability in SND and
67 snow cover extent over the Arctic terrestrial regions during 1948–2006, based on a simulation
68 by the land surface model CHANGE (Park et al., 2011a). Here we extend the previous study,
69 combining it with observational data for SIE.
70
71 2. Model Description

72 CHANGE is a state-of-the-art process-based model of the land surface. It calculates
73 heat, water, and radiation fluxes over soil, canopy, and snow surfaces in the atmosphere-land
74 system, as well as soil thermal and hydrologic states, including an explicit treatment of soil
75 freeze/thaw phase changes, and carbon and nitrogen fluxes in ecosystems. Permafrost

dynamics were improved by representing the effects of soil organic matter changes with time, depending on the simulated soil carbon budget according to soil thermal and hydrological properties. Soil depth was extended to 30.5 m to capture the thermal inertia provided by deep ground, considering a vertically heterogeneous soil texture distribution. Evapotranspiration was calculated as the sum of partitioned transpiration, interception, and soil evaporation. Transpiration was greatly dependent on variations in the leaf area index and root amounts, for which the spatiotemporal variations were also simulated by the model for every time step.

The CHANGE model represents snow dynamic processes using a two-layer energy and mass balance approach. The energy balance is used to simulate snowmelt, refreezing, and changes in the snowpack heat content. In calculating the radiation balance, the shortwave radiation is divided into direct beam and diffuse radiation because the canopy and soil have different spectral properties for individual spectral bands. The albedo for the canopy and soil is also calculated by a two-stream approximation method, in which the ground albedo for the two components is determined by weighting the soil and snow albedos. The mass balance components represent snow accumulation/ablation, changes in snow water equivalent, and water yield from the snowpack. The snowpack compacts with snowfall, which increases gravitational settling and also contributes to the densification of the snowpack. Therefore, compaction represents the sum of metamorphism and overburden, which also influences snow density. The estimated snow density along with the simulated snow water equivalent is used to estimate snow depth. A part of snowfall is primarily intercepted by the canopy when overstory is present. The processes of snow interception are calculated by the algorithm of Storck et al. (2002). The CHANGE model incorporates a vegetation dynamics model, which is useful to assess the effect of changing vegetation structure on the land surface processes. Park et al. (2011a) provided a full description of the CHANGE model.

3. Datasets

We forced the CHANGE model with a gridded climate dataset of 0.5° latitude/longitude and daily resolutions over the global land area for the period 1948–2006. Because the dataset was extensively described by Hirabayashi et al. (2008) and Park et al. (2011b), only a brief description is provided here. The gridded products for air temperature and precipitation (P_G) were interpolated based on various monthly station observations. The temperature data were obtained from the Climatic Research Unit (CRU) Ts 2.1, the Global Historical Climatology Network (GHCN), and the NOAA Climate Prediction Center (CPC) Climate Anomaly Monitoring System (CAMS) datasets, and P_G data were obtained from NOAA CPC station data and the Global Precipitation Climatology Centre (GPCC) ver. 5. A stochastic weather generator was used to disaggregate monthly climatic variables into a daily time series. The daily shortwave radiation was derived from the surface radiation budget (SRB). The wind speed was obtained from the European Centre for Medium-Range Weather Forecasts (ECMWF) 40-year reanalysis (ERA-40); the wind speed at 2.5° resolution was interpolated to 0.5° grids within the 2.5° × 2.5° grid.

Initial conditions for the soil thermal and hydrological regimes and vegetation components were determined by a spin-up, running from an assumed state of no snow, no soil carbon, and a prescribed minimum of vegetation carbon. The soil moisture was initially set to the field capacity of the soil type for the top 5.5 m depth and to 90% of saturation for the remaining layers, and the vertical distribution of soil temperature was linearly interpolated using the air temperature at the simulation start date and annual mean temperature. The spin-up was run for approximately 420 years by looping repeatedly through a record of the initial 20 years of meteorological data. Total ecosystem carbon was used as a primary diagnostic for the spin-up run. The total ecosystem carbon was averaged over the 20-year period for each cycle. As the trend in the averaged total ecosystem carbon over time reached a threshold value (0.1 g C/m^2/yr), the spin-up was completed. Any influences of the initial

126 conditions on the other processes were generally offset during the spin-up. The CHANGE
127 model does not include glaciers yet, and thus Greenland was excluded from the simulation.
128 The whole land region ＞45°N was set for the simulation.

129 The SIE data retrieved from the Scanning Multichannel Microwave Radiometer
130 and the Special Sensor Microwave/Imager using the NASA team algorithm (Fetterer et al.,
131 2002) were obtained from the National Snow and Ice Data Center (NSIDC). A SIE data set is
132 available at a spatial resolution of 25 km; but we used the mean SIE time series available
133 from the NSIDC Sea Ice Index (http://nsidc.org/data/seaice_index/).

134 We also used the Climate Research Unit (CRU) air temperature and P_G data sets,
135 version 3.0 (http://www.cru.uea.ac.uk/cru/data/hrg/), which consist of land-based monthly
136 data on a regular 0.5° longitude/latitude global grid. The CRU data were used to investigate
137 the influences of decreasing SIE on land surface temperature and P_G for the study period and
138 the subsequent effect on SND.

139

140 4. Results

141 4.1 Sea ice extent and climate

142 A diminishing SIE for the period of the available satellite data record was
143 conspicuous in all months, with the minimum extent typically occurring in September. Both
144 the actual and detrended ice extents are shown in Fig. 1. The detrended values exclude effects
145 of the interannual variability in ice extent alone. The SIE decreased about 21.3% ($p < 0.0001$
146 by Mann-Kendall test) during the period of 1979–2006. The rate of retreat for SIE outpaced
147 the projections simulated by Intergovernmental Panel on Climate Change Fourth Assessment
148 Report (IPCC AR4) climate models in response to greenhouse warming (Stroeve et al., 2007).
149 An extreme decline in sea ice cover since 2005 was found in an extended region (the
150 Beaufort Sea, Chukchi Sea, East Siberian Sea, Laptev Sea, and Kara Sea) compared with the

151 ice edge for the minimum conditions averaged over 1979–2006. The SIE was at a minimum
152 in 2007 and declined further in the East Siberian Sea compared with 2005; however, it
153 recovered in the Sea around the Taymyr Peninsula (e.g., Comiso et al., 2008). When the
154 amount of highly reflective sea ice is reduced, the input of solar heat into the ocean is
155 increased, leading to increases in heat storage in the upper ocean. As a result, the warm upper
156 ocean retards the recovery of sea ice coverage in autumn and early winter. Furthermore,
157 during this period the anomalously warm, ice-free ocean water enhances the heat and
158 moisture fluxes between the surface and atmosphere, which are extended to the terrestrial
159 Arctic with implications for atmospheric circulation (Screen and Simmonds, 2010).

160 The Arctic Oscillation (AO), which is a leading mode of wintertime climate
161 variability in the Northern Hemisphere, has exhibited a decreasing trend since 1988 ($p <$
162 0.032) (Fig. 1). The AO is closely correlated to Eurasian snow cover in the autumn, with a
163 higher autumn snow cover generally leading to a negative AO in the lower troposphere in
164 winter (Cohen et al., 2007). The negative AO trend favors anomalously cold temperatures
165 over the eastern United States and northern Eurasia in winter (Thompson and Wallace, 1998).

166 The wintertime (December–February) surface air temperature (SAT) during
167 1979–2006 exhibited a dipole pattern in its trend between Eurasia (EUR) and North America
168 (NA) (Fig. 2a). Winter warming was significant over most of NA except for western Alaska,
169 and the magnitude of the warming tended to be larger in the northern regions than in the
170 south. The maximum increase in SAT over NA was found in eastern Alaska with a warming
171 trend of 1.6℃/decade. SAT in the Scandinavian Peninsula also exhibited a strong increasing
172 trend. However, conspicuous negative trends were identified over far eastern and
173 north-central Siberia. Interestingly, the trend of SAT in EUR also revealed large magnitude
174 changes in the northern regions, as in NA. Precipitation exhibited regionally heterogeneous
175 trends (Fig. 2b). In NA, significant trends of P_G were found at the western seashore regions

and eastern Canada. In EUR, P_G trends showed clear differences between the eastern and western regions. Western EUR exhibited a strong decrease with locally positive trends, whereas eastern EUR generally retained the normal state of P_G, with the exception of the Far East.

4.2 Snow depth variability

The averaged snow depth during winter in both NA and EUR indicated a decreasing trend, which was statistically significant only in NA (Fig. 3). From 1954 to the early 1970s, both continents retained a value of SND considered to be above normal. Thereafter, SND in EUR decreased and then continued a pattern of normal anomalies until 2000, when it began to decrease again. In NA, SND exhibited an obvious decreasing trend ($p < 0.0001$) from 1971 onward. The decrease in the 1990s and 2000s was particularly strong, reaching a maximum of 10 cm in 1997. Dyer and Mote (2006) recorded a locally significant decrease (-0.25 cm yr^{-1}) in the SND of northwestern Canada, in response to rising air temperature, during the period of 1960–2000. The maximum SND in the western prairie provinces of Canada also decreased by 31–64% during the period of 1956–2003 (Schindler and Donahue, 2006). On the other hand, *in situ* observations in EUR have shown increasing trends of winter SND (Bulygina et al., 2009; Kitaev et al., 2005), which is contrary to our result. The period of 1979–2006, for which satellite SIE data are available, also exhibited statistically significant decreasing trends in SND for both NA ($p < 0.0004$, slope = -0.21) and EUR ($p < 0.02$, slope = -0.08) (Fig. 3).

Monthly SND data for EUR and NA show evident decreases during the past two decades (Fig. 4a, b). The decreases are stronger in NA than in EUR. In NA, the negative trend in most months during the period of 1979–2006 was at least twice as large as during the

1948–2006 period. The largest decreases were identified during the winter months (i.e., December–March), which was likely to be a combined effect of increased SAT (Fig. 4f) and less P_G (Fig. 4h). The increase in SAT in January–March during the 1979–2006 period was lower than that during the 1948–2006 period (Fig. 4f). In spite of such temperature conditions, SND decreased substantially, which seems to be related to the lower P_G (Fig. 4h). The negative trend of SND in April was the largest (i.e., 2.3 cm/decade), which was also influenced by a higher SAT (Fig. 4f) and less P_G (Fig. 4h). Satellite and *in situ* observations have revealed reductions in spring snow cover over NA during recent decades (Brown et al., 2010). On the other hand, the autumnal P_G in NA increased (Fig. 4h), while SND decreased, which was also associated with the warm SAT (Fig. 4f).

In EUR, SND also exhibited negative trends in most months during the two periods, with the exception of November, which had a positive trend (Fig. 4c). SAT also increased (Fig. 4e), as it did in NA. However, the magnitude of the decrease in SND was considerably lower than in NA (Fig. 4d), probably as a result of the increased P_G in the autumn and winter (Fig. 4g). While the SND trends in November–January during the 1979–2006 period were statistically significant, no statistical significance was found for the trends of SAT and P_G in the autumn and winter months of the same period.

The SND during 1979–2006 shows large heterogeneous spatial trends for autumn (Fig. 5a) and winter (Fig. 5b). In autumn, the region where the trend of SND was significant (either positive or negative) was concentrated in the northernmost regions $>60°$N. In EUR the regions with a positive trend were widespread, while the trend in NA was generally negative. The increase in SND over Siberia (Fig. 5a) was consistent with the spatial patterns suggested by Bulygina et al. (2009), who documented an increase in the duration of snow cover over central Siberia and the Far East. In the winter, the areas with a negative trend in SND increased in both EUR and NA (Fig. 5b). Particularly in southwestern Canada, where

225 the trend of SND in the autumn was positive, there was a change to a strong negative trend
226 that was statistically significant. In northern EUR, the area with a positive trend in winter
227 SND also reduced relative to the autumn, and the negative trend of SND in northern Europe
228 was further strengthened. By contrast, areas with a positive trend in SND increased over
229 southern Siberia.
230
231 4.3 The influence of diminishing Arctic sea ice on snow depth
232 After summers with a below-normal SIE, the fluxes of heat and moisture from the
233 sea surface to the atmosphere are anomalously large (Francis et al., 2009). The additional
234 heat transfer into the atmosphere leads to strong stability in the lower atmosphere, which
235 limits vertical mixing (Francis et al., 2009; Screen and Simmonds, 2010). The Arctic
236 warming was greatest in autumn and winter, and signals of this warming were not confined to
237 the sea but also extended to the Arctic boreal regions (Screen and Simmonds, 2010). The
238 composite differences in autumn mean air temperatures after summers when the SIE was less
239 than, and greater than, one standard deviation from the mean of the 1979–2006 period (Fig.
240 1) are shown in Fig. 6(a) and 6(d). Using the actual SIE, the composites reveal large areas
241 with positive temperature differences over the Arctic land surface (Fig. 6a). The largest
242 differences exceeding 3°C were found over far eastern Siberia, western Alaska, and the
243 Canadian Archipelago. These areas belong to the Pacific and Atlantic marginal ice zones,
244 where ice loss has been most pronounced (Liu et al., 2012). The composite analysis, using
245 detrended ice extents, replaced most regions of positive temperature differences with negative
246 values, with the exception of Alaska (Fig. 6d). This was particularly significant for the
247 ambient regions of Hudson Bay and north-central Siberia, where the maximum difference
248 was 5°C or more. This result suggests that the response in these regions is a symptom of the
249 large-scale warming tendency related to the SIE trend (Francis et al., 2009).

250 Increases in atmospheric water vapor are related to the sea ice loss and enhance the
251 warming in the lower part of the atmosphere during summer and early autumn (Screen and
252 Simmonds, 2010). An increase in the atmospheric water vapor content enhances the emission
253 of longwave radiation to the surface (Francis et al., 2009), resulting in surface warming. The
254 warming would in turn be expected to affect large-scale atmospheric circulation and
255 ultimately influence the weather of the Arctic region. This is evident from the composite
256 differences in the autumnal P_G during reduced-versus-extensive ice years, with and without
257 the trends in ice extent (Fig. 6b and 6e). The composite differences using the actual SIE trend
258 identified the increase in autumnal P_G over much of the terrestrial Arctic (Fig. 6b), when
259 compared to the composites using the detrended ice extents (Fig. 6e). The increase in the
260 autumnal P_G was significant in the ambient regions of Hudson Bay, central Siberia, and
261 western EUR (Fig. 6b). The increase appears to be associated with the trend of ice extent.
262 Recent studies have linked decreasing sea ice to increases in autumn cloud cover over the
263 Arctic (Levinson and Lawrimore, 2008) and in precipitating clouds over Siberia (Eastman
264 and Warren, 2010; Stroeve et al., 2011). Modeling studies (Ghatak et al., 2010; Orsolini et al.,
265 2011) have also illustrated that the reduction in sea ice can increase autumnal snowfall over
266 Siberia (Fig. 5a). Interestingly, the increase in P_G in eastern Canada and western EUR is
267 reminiscent of the North Atlantic Oscillation (NAO) (Hurrel, 1995). When the NAO index is
268 in a positive phase, the pressure difference in the northeastern Atlantic is large, consequently
269 increasing storm frequency (Francis et al., 2009).
270 The composite differences in autumnal SND over northern Siberia were positively
271 anomalous when using actual (Fig. 6c) or detrended (Fig. 6f) ice extents. The magnitudes of
272 the composite differences in SND were larger over much of the Arctic land surface when the
273 trend of SIE was not included (Fig. 6f). In contrast, when the actual trend was considered, the
274 area of the positive anomaly in SND over Siberia decreased. This means that the warming

275 associated with the reduced ice extent contributed to the decrease in SND, which was
276 significant for northern Canada and western and far eastern Siberia, where the response of
277 temperature to sea ice loss was substantial (Fig. 6a). For example, in northeastern Canada, the
278 difference in SND using the detrended ice extent was ＋10 cm or more (Fig. 6f), whereas
279 using the actual ice extent it was −4～0 cm (Fig. 6c). Higher temperatures would primarily
280 increase the fraction of rainfall, rather than snowfall, when precipitation occurs, and would
281 ultimately retard the accumulation of snow. Simulations by Park et al. (2011b) indicated that
282 the timing of the onset of snow over the Arctic land surface was delayed by a maximum of
283 eight days since 1989, due to the warming temperatures. Furthermore, warming increases
284 sublimation from the snow surface, consequently decreasing SND. SND in Alaska exhibited
285 the strongest negative differences when using both actual (Fig. 6c) and detrended (Fig. 6f) ice
286 extents, which seems to be associated with the higher temperatures (Fig. 6a and d).

287 The memory mechanism that extends the influence of the reduced ice extent into
288 winter has previously been explained by several studies (Deser et al., 2007; Francis et al.,
289 2009; Peng and Whitaker, 1999). The heating of the lower atmosphere associated with the sea
290 ice loss increases the vertical thickness of the lower troposphere, which results in higher
291 geopotential heights of the ice-free upper pressure surfaces and reduces the poleward
292 temperature gradient between the mid- and high latitudes. A reduction of SIE-induced
293 influences on winter weather were found in the linear regressions of inverted SIE with SAT,
294 P_G, and SND during the following winter, where the trended (Fig. 7, top) and detrended (Fig.
295 7, middle) SIEs in September were used. The regression values represent changes in variables
296 corresponding to a one million-km^2 change in SIE. The regression indicated that the actual
297 SIE resulted in warming in NA and cooling in EUR (Fig. 7a). Conversely, when the trend of
298 SIE is removed, an increase in the winter SAT occurred over far eastern Siberia, while cold
299 air developed over eastern NA and the Scandinavian Peninsula (Fig. 7d). Temperature

300 anomalies in central Siberia were 2–3℃ below normal, in association with the SIE decrease
301 (Fig. 7a and d). The increase in SAT in northeastern Canada and Greenland was influenced
302 by incursions of warm air masses from the North Atlantic in association with low ice
303 coverage (Liu et al., 2012). The regression of winter SAT anomalies onto the winter AO (Fig.
304 7g) produced a completely different map from that of the actual SIE (Fig. 7a). The dipole
305 anomalies of warm SAT over NA and cold SAT over EUR (Fig. 7g) resemble the classical
306 negative trend of the AO pattern (Thompson and Wallace, 2001), which is forced partly by
307 the increase in Eurasian snow cover during autumn (Cohen et al., 2007).

308 The regression between AO and P_G indicates higher positive values over
309 northeastern Canada, southern Europe, and far eastern Siberia. The remaining regions
310 exhibited negative or weak positive regressions (Fig. 7h). The influence of SIE on P_G was
311 similar in the two regressions (Fig. 7b and e). However, it tends to result in a higher P_G over
312 the Canadian region when the trend of SIE is removed (Fig. 7e). The reduction in sea ice
313 produced a zone of wet winters from the seashore of the Sea of Okhotsk across the southern
314 seashore of Alaska, over southern Canada to western EUR (Fig. 7b and e). This pattern of P_G
315 was similar to the North Pacific pattern. Meanwhile, areas of negative anomalies were
316 evident over southern Hudson Bay, northern Europe, and southeastern EUR (Fig. 7b and e).

317 A regression of SIE with winter SND (Fig. 7c) was similar to the P_G regression
318 (Fig. 7b). However, the SND variability is complicated as increases in P_G also contribute to
319 greater SND. This is because the increased temperature associated with sea ice loss can
320 readily offset the impact of P_G on SND. The actual effects of the higher temperatures were
321 observed in the decreased SND in Alaska and southern Canada (Fig. 7c). The decreased SIE
322 resulted in a significant increase in SND in northeastern Siberia (Fig. 7c), where SND
323 anomalies were up to 8 cm above normal in association with a one million km^2 decrease in
324 the SIE. The detrended SIE resulted in a significant increase in SND over the Canadian

325 region, excluding the Arctic islands (Fig. 7f). An increase in SND anomalies was also found
326 over western EUR (Fig. 7f). The regression indicated an increase in SND over eastern Siberia
327 (Fig. 7f), as shown in Fig. 7(c), which suggests that SND in the region is closely correlated
328 with the reduction of SIE.

329 Recent studies have suggested that the negative trend in the AO is correlated to
330 decreasing Arctic sea ice (Overland and Wang, 2010; Petoukhov and Semenov, 2010).
331 Associated with the AO, there is increased SND during winter over much of the southern
332 Arctic land surface, particularly southwestern Canada and south-central Siberia (Fig. 7i),
333 which contrasts noticeably with the regression of SIE onto winter SND shown in Fig. 7(c).
334 This difference was expected because the decrease in autumn SIE clearly indicates
335 differences in the interannual variability relative to the winter AO (Fig. 1), and the winter AO
336 and the detrended SIE are weakly correlated (0.17). Interestingly, the regression of AO with
337 SND (Fig. 7i) is reminiscent of that expected for negative AO patterns; for example, when the
338 winter AO has a negative trend, the frequency of storms in the middle latitudes is increased
339 (Thompson and Wallace, 2001).

340

341 5. Discussion

342 As illustrated in Fig. 7(c), the contribution of the reduction in SIE to the increase in
343 SND was evident for the northernmost terrestrial regions, matching the regions where P_G
344 regressed with SIE was positively anomalous (Fig. 7b). The rapid retreat of sea ice in summer
345 and the slow ice growth during autumn enhanced the latent heat flux from the ocean surface
346 to the atmosphere (Screen and Simmond, 2010), increasing lower tropospheric moisture over
347 the Arctic, which combines with the effect of the Clausius-Clapeyron relationship to enhance
348 the likelihood of anomalous snowstorm events. The increase in available moisture could
349 potentially lead to higher precipitation efficiency over the Arctic. The reduction in SIE

350 contributed to the increase in autumnal P_G over much of the terrestrial Arctic (Fig. 6b), which
351 was linked to higher SND (Fig. 6c). Finnis et al. (2007) indicated that high-latitude regions
352 experience increased P_G from storms during autumn owing to the availability of atmospheric
353 moisture associated with the diminishing sea ice. The diminished sea ice in turn recovers
354 during late autumn and early winter. During the ice recovery, the humidity of the Arctic air
355 masses increases, which may be connected to the variability of winter P_G over the Arctic. A
356 recent study noted that the declining Arctic sea ice is directly connected to a shift to a more
357 meridional atmospheric circulation pattern in winter, rather than zonal symmetry (Liu et al.,
358 2012). The modified circulation pattern transports the moisture induced in autumn southward
359 from the Arctic. Kurita (2011), using water isotopes as tracers, found that water vapor in
360 eastern Siberia during ice growth originated from the Arctic Ocean. Observational data have
361 also shown that following an anomalously low ice extent in autumn, a pronounced increase in
362 humidity occurred in far eastern Siberia, northern/eastern Europe, and western Alaska (Liu et
363 al., 2012). The increased humidity would provide moisture sources to the regions, resulting in
364 higher SND. This suggests that a first-order link between sea ice variability and winter P_G
365 potentially contributes to SND variability, through the changed circulation pattern.
366 The detrended SIE resulted in strong increases in winter SND over large parts of
367 Canada (Fig. 7f), which was clearly distinguished from the negative trend of SND (Fig. 5b).
368 In particular, the increase in SND in western Canada was associated with P_G patterns
369 modified by the reduction in Arctic sea ice. Western Canada is known to be influenced by a
370 moisture influx associated with the Aleutian low. Francis et al. (2009) noted that the Aleutian
371 low during autumn was weaker following summers with less ice. However, intraseasonal
372 modeling studies have suggested that as Arctic sea ice cover is reduced, precipitation patterns
373 over western NA shift toward drier conditions in southwestern NA and wetter conditions in
374 northwestern NA (Sewall, 2005). In reality, increases in P_G in western Canada were identified

375 during autumn (Fig. 6b) and winter (Fig. 7e) and are responsible for the increase in winter
376 SND over Canada (Fig. 7f), which differs from the general negative trend of SND (Fig. 5b).
377 The diminishing Arctic sea ice has simultaneously contributed to the increase in
378 SAT (Serreze and Francis, 2006; Serreze et al., 2009) alongside the increase in P_G (Fig. 7b).
379 The increase in winter SAT over northwestern NA was remarkably significant (Fig. 2b and
380 Fig. 4f) relative to the cold Siberia region (Fig. 6a). The variability of SND is sensitive to the
381 radiative balance (Groisman et al., 1994), surface energy fluxes (Dyer and Mote, 2002), and
382 variations in air temperature (Brown and Goodison, 1996). The increased SAT can
383 overwhelm the effect of the increased P_G (Fig. 4), thereby decreasing SND. Under warming
384 conditions, snowfall is partially or wholly replaced by rain, and snowmelt is increased,
385 resulting in a diminished snowpack. A significant decrease in SND over northwestern Canada
386 in response to rising air temperatures has been observed (Dyer and Mote, 2006). Park et al.
387 (2011b) have also suggested the influence of warming temperatures on the negative trend in
388 winter SND over much of NA. The Community Climate System Model (CCSM3) future
389 simulations showed reductions of snow cover at the hemispheric scale outside the Siberian
390 region, which correlated with the reduction of Arctic sea ice (Ghatak et al., 2010).
391 The SND in eastern Siberia increased during autumn (Fig. 5a) in response to the
392 reduction in sea ice, and these SND conditions continued throughout the winter season (Fig.
393 7c). Larger snow depth over Siberia was also identified by future simulation experiments.
394 Global climate models have projected an increase in snow water equivalent over northern
395 Siberia, responding to sea ice loss in the 21st century (Callaghan et al., 2011; Deser et al.,
396 2010; Räisänen, 2008). Although temperature has increased, the Siberian regions are
397 sufficiently cold to maintain snow cover during the winter season (Fig. 7a). The cold winter
398 in Siberia is closely related to the aforementioned circulation changes. Under the diminishing
399 Arctic sea ice conditions, the weakened westerly winds tend to exhibit broad meanders that

400 are likely to form blocking circulations in Eastern Europe, central Siberia, and southern
401 Alaska. Such blocking favors more frequent incursions of cold air masses from the Arctic
402 into the middle and low latitudes of northern continents (Liu et al., 2012). In these cold
403 conditions, a more moisture-laden atmosphere, resulting from sea ice loss in autumn,
404 contributes to the increase in snowfall.

405 Snow is a strong insulator, limiting heat transfer between the atmosphere and the
406 ground. The variability of SND during the early winter can either amplify or mitigate soil
407 warming, which is likely to persist into the following summer as a memory in the soil system.
408 To explore the insulation effect, the detrended mean SND during September–November was
409 linearly regressed with the mean soil temperature at 1.2 m of the following summer (i.e.,
410 June–August) over the 1979–2006 period (Fig. 8). The investigation was limited to the
411 permafrost area as defined by the model. Strong insulation effects of SND on soil
412 temperature were discovered over east Siberia, where SND in autumn exhibited an increasing
413 trend (Fig. 5a). The insulation effect reached a maximum of 0.2℃ or more per 1 cm SND in
414 south Siberia. The corresponding value in northeastern Siberia was 0.10–0.15℃. In NA, a
415 positive relationship between autumnal SND and soil temperature was determined in the
416 northernmost regions; for example, soil temperature in the Canadian Arctic increased by
417 0.06–0.14℃ per 1 cm SND. By contrast, the reduced SND in western Alaska resulted in soil
418 cooling. Soil temperature in southern Canada, with a lower, SND increased, while in central
419 Siberia, it was negatively regressed with the higher autumnal SND (Fig. 5a). It seems that the
420 negative anomalies of soil temperature in central Siberia were associated with the cold air
421 temperature (Fig. 2a) and the reduced SND (Fig. 5b) during the subsequent winter season.
422 Likewise, an increase or decrease in SND was not necessarily connected to soil warming or
423 cooling (as shown in Fig. 8) because soil temperature has a complex relationship with air

424 temperature, precipitation, and soil moisture during the subsequent winter and next summer
425 season. Park et al. (2012) also found that the influence of soil moisture on the thermal state of
426 summer soil can override the effect of air temperature. However, there was an evident
427 empirical relationship, where the increased SND was tied to soil warming, at least in eastern
428 Siberia and the Canadian Arctic, suggesting that the role of decreasing sea ice is behind the
429 relationship between SND and soil temperature. Lawrence and Slater (2010) suggested that
430 for the latter half of the twentieth century, snow state variations explain as much as 50–100%
431 of total soil temperature variations. In a future SIE experiment for Alaska, snowpack in the
432 winter season increased significantly, which contributed to warmer soil temperatures for most
433 seasons by insulating the land surface (Higgins and Cassano, 2012).
434
435 6. Conclusion
436 In this study, we evaluated how the diminishing SIE in September has influenced
437 SND over Arctic terrestrial regions during the period of 1979–2006. During this period, the
438 Arctic sea ice in September continuously decreased, and the simulated SNDs in EUR and NA
439 also produced decreasing trends. The decrease in SND was more significant in NA than in
440 EUR and was closely correlated to temperature warming. Regional increases in SND were
441 found in eastern Siberia, northern Alaska, and the Canadian Arctic amid the reduction in
442 Arctic sea ice. Diminishing Arctic sea ice contributed to the increase in P_G, which was linked
443 to snowy winters over large parts of the northern terrestrial Arctic. Furthermore, linear
444 regression of detrended SIE with SND indicated that the reduction in sea ice resulted in a
445 positively anomalous SND in eastern Siberia, as well as Canadian regions where a negative
446 trend of SND was clear. This study demonstrates that diminishing sea ice definitely affected
447 SND in the northernmost terrestrial regions.
448 Regional responses of SAT to reductions in Arctic sea ice were quite different.

449 Temperature in northwestern NA increased anomalously with diminishing sea ice. The
450 warming temperatures over NA overwhelmed the effect of increased P_G, thereby decreasing
451 SND. By contrast, the reduction in sea ice led to cold conditions over Siberian regions in
452 winter. Together with enhanced snowfall, this contributed to an increase in SND in eastern
453 Siberia. The thicker SND in eastern Siberia early in the snow season was linked to soil
454 warming in the following summer. The insulation effect of SND on soil temperature was also
455 found in part of the Canadian Arctic.

456 Episodes of diminishing sea ice, which have increased SND over eastern Siberia,
457 have been suggested by recent observations and climate modeling results. This study also
458 identified such an episode in the Canadian Arctic. We can conclude definitively that
459 diminishing Arctic sea ice has increased SND in the northernmost terrestrial Arctic during
460 recent decades. The decrease in snow depth on a continental scale, outside of the
461 northernmost regions, suggests a sea ice-related Arctic amplification on the terrestrial Arctic
462 snowpack. If the decline of Arctic sea ice continues as anticipated by global climate models,
463 we can speculate that the variability of terrestrial Arctic snow will intensify, along with
464 warming temperatures and more persistent snowstorms during winter. A better understanding
465 of interactions between the diminishing Arctic sea ice and winter mean statistics (i.e., snow
466 and temperature) is an important area for further research.

467

468 Acknowledgment

469 This study was supported as a collaboration theme between the Japan Agency for
470 Marine-Earth Science and Technology (JAMSTEC) and the International Arctic Research
471 Center (IARC), University of Alaska, Fairbanks.

472

473 References

474 Bekryaev, R., Polyakov, I. Alexeev, V., 2010. Role of polar amplification in long-term
475 surface air temperature variations and modern Arctic warming. J. Clim. 23,

476 3888-3906, doi:10.1175/2010JCLI3297.1.
477 Brown, R., 2000. Northern Hemisphere snow cover variability and change, 1915-97.
478 J. Clim. 13, 2339–2355,
479 doi:10.1175/1520-0442(2000)013<2339:NHSCVA>2.0.CO;2.
480 Brown, R., Goodison, B., 1996. Interannual variability in reconstructed Canadian snow
481 cover. 1915–1992. J. Clim. 9, 1299–1318.
482 Brown, R., Derksen, C., Wang, L., 2010. A multi-data set analysis of variability and
483 change in Arctic spring snow cover extent, 1967-2008. J. Geophys. Res. 115,
484 D16111, doi:10.1029/2010JD013975.
485 Bulygina, O., Razuvaev, V., Korshunova, N., 2009. Change in snow cover over northern
486 Eurasia in the last decades. Environ. Res. Lett. 4, 045026,
487 doi:10.1088/17489326/14/4/045026.
488 Callaghan, T., Johansson, M., Brown, R., Groisman, P., Labba, N., Radionov, V., 2011.
489 Changing snow cover and its impacts, in AMAP, 2011, Snow, Water, Ice and
490 Permafrost in the Arctic (SWIPA): Climate Change and the Cryosphere, Arctic
491 Monitoring and Assessment Programme (AMAP), Oslo, Norway, 538 pp, 2011.
492 Cohen, J., Barlow, M., Kushner, P., Saito, K., 2007. Stratosphere-troposphere coupling and
493 links with Eurasian land-surface variability. J. Clim. 20, 5335–5343.
494 Cohen, J., Furtado, J., Barlow, M., Alexeev, V., Cherry, J., 2012. Arctic warming, increasing
495 snow cover and widespread boreal winter cooling. Environ. Res. Lett. 7, 014007,
496 doi:10.1088/1748-9326/1/1/014007.
497 Comiso, J., Parkinson, C., Gersten, R., Stock, L., 2008. Accelerated decline in the Arctic sea
498 ice cover. Geophys. Res. Lett. 35, L01703, doi:10.1029/2007GL031972.
499 Deser, C., Thomas, R., Peng, S., 2007. The transient atmospheric circulation response to
500 North Atlantic SST and sea ice anomalies. J. Clim. 20, 4751–4767.
501 Deser, C., Tomas, R., Alexander, M., Lawrence, D., 2010. The seasonal atmospheric
502 response to projected Arctic sea ice loss in the late twenty-first century. J. Clim. 23,
503 333–351, doi:10.1175/2009JCLI3053.1.
504 Dyer, J., Mote, T., 2002. Role of energy budget components on snow ablation from a
505 mid-latitude prairie snowpack. Polar Geogr. 26, 87–115.
506 Dyer, J., Mote, T., 2006. Spatial variability and trends in observed snow depth over
507 North America. Geophys. Res. Lett. 33, L16503, doi:10.1029/2006GL027258.
508 Eastman, R., Warren, S., 2010. Interannual variations of Arctic cloud types in relation to sea

509 ice. J. Clim. 23, 4216–4232.
510 Fetterer, F., Knowles, K., Meier, W., Savoie, M., 2002. Sea Ice Index (National Snow and Ice
511 Data Center, Boulder, CO) (updated 2009).
512 Finnis, J., Holland, M., Serreze, M., Cassano, J., 2007. Response of Northern Hemisphere
513 extratropical cyclone activity and associated precipitation to climate change, as
514 represented by the Community Climate System Model. J. Geophys. Res. 112,
515 G04S42, doi:10.1029/2006JG000286.
516 Francis, J., Chan, W., Leathers, D., Miller, J., Veron, D., 2009. Winter Northern Hemisphere
517 weather patterns remember summer Arctic sea-ice extent. Geophys. Res. Lett. 36,
518 L07503, doi:10.1029/2009GL037274.
519 Ghatak, D., Frei, A., Gong, G., Stroeve, J., Robinson, D., 2010. On the emergence of an
520 Arctic amplification signal in terrestrial Arctic snow extent. J. Geophys. Res. 11,
521 D24105, doi:10.1029/2010JD014007.
522 Groisman, P., Karl, T., Knight, R., 1994. Changes of snow cover, temperature, and
523 radiative heat balance over the Northern Hemisphere. J. Clim. 7, 1633–1656.
524 Higgins, M., Cassano, J., 2012. Northern Alaskan land surface response to reduced Arctic sea
525 ice extent. Clim. Dyn. 38, 2099-2113, doi:10.1007/s00382-011-1095-0.
526 Hirabayashi, Y., Kanae, S., Motoya, K., Masuda, K. Doll, P., 2008. A 59-year (1948-2006)
527 global near-surface meteorological data set for land surface models. Part I:
528 Development of daily forcing and assessment of precipitation intensity. Hydrol.
529 Res. Lett. 2, 36-40.
530 Hurrell, J., 1995. Decadal trends in the North Atlantic Oscillation: Regional temperatures and
531 precipitation. Science 269, 676-679.
532 Intergovernmental Panel on Climate Change (IPCC), 2008. Climate Change 2007: Synthesis
533 Report. Contribution of Working Groups I, II and III to the Fourth Assessment
534 Report of the Intergovernmental Panel on Climate Change, edited by Core Writing
535 Team et al., 104 pp., Geneva, Switzerland.
536 Kitaev, L., Forland, E., Razuvaev, V., Tveito, O., Krueger, O., 2005. Distribution of snow
537 cover over Northern Eurasia. Nord. Hydrol. 36, 311–319.
538 Kurita, N., 2011. Origin of Arctic water vapor during the ice-growth season, Geophys. Res.
539 Lett. 38, L02709, doi:10.1029/2010GL046064.
540 Lawrence, D., Slater, A., 2010. The contribution of snow condition trends to future ground
541 climate. Clim. Dyn. 34, doi: 10.1007/s00382-009-0537-4.

542 Levinson, D., Lawrimore, J., 2008. State of the Climate in 2007. Bull. Am. Meteorol. Soc.
543 89, S1–S179, doi: 10.1175/BAMS-89-7-StateoftheClimate.
544 Liu, J., Curry, J., Wang, H., Song, M., Horton, R., 2012. Impact of declining Arctic sea ice on
545 winter snowfall. Proc. Natl. Acad. Sci. USA. doi:10.1073/pnas.1114910109.
546 McCabe, G., Wolock, G., 2010. Long-term variability in Northern Hemisphere snow cover
547 and associations with warmer winters. Clim. Change 99, 141–153,
548 doi:10.1007/s10584-009-9675-2.
549 Orsolini, Y., Senan, R., Benestad, R., Melsom, A., 2011. Autumn atmospheric response to
550 the 2007 low Arctic sea ice extent in coupled ocean-atmosphere hindcasts. Clim.
551 Dyn. 114, D19108, doi:10.1007/s00382-011-1169-z.
552 Overland, J., Wang, M., 2010. Large-scale atmospheric circulation changes are associated
553 with the recent loss of Arctic sea ice. Tellus A, 62, 1–9.
554 Park, H, Iijima, Y., Yabuki, H., Ohta, T., Walsh, J., Kodama, Y., Ohata, T., 2011a. The
555 application of a coupled hydrological and biogeochemical model (CHANGE) for
556 modeling of energy, water, and CO_2 exchanges over a larch forest in eastern Siberia.
557 J. Geophys. Res. 116, D15102, doi:10.1029/2010JD015386.
558 Park, H., Yabuki, H., Ohata, T., 2011b. Analysis of satellite and model datasets for variability
559 and trends in Arctic snow extent and depth, 1948–2006. Polar Sci.
560 doi:10.1016/J.polar.2011.11.002.
561 Park, H., Walsh, J., Fedorov, A., Sherstiukov, A., Iijima, Y., Ohata, T., 2012. The influence
562 Of climate and hydrological variables on opposite anomaly in active layer thickness
563 Between Eurasian and North American watersheds. The Cryosphere Discuss. 6,
564 1–38, doi:10.5194/tcd-6-1-2012.
565 Peng, S., Whitaker, J., 1999. Mechanisms determining the atmospheric response to
566 midlatitude SST anomalies. J. Clim. 12, 1393–1408.
567 Peterson, B. *et al*., 2002. Increasing river discharge to the Arctic Ocean. Science 298,
568 2171–2173, doi:10.1126/science.1077445.
569 Petoukhov, V., Semenov, V., 2010. A link between reduced Barents-Kara sea ice and cold
570 winter extremes over northern continents. J. Geophys. Res. 115, D21111,
571 doi:10.1029/2009JD013568.
572 Räisänen, J., 2008. Warmer climate: less or more snow? Clim. Dyn., 30, 307–319, doi:
573 10.1007/s00382-007-0289-y.
574 Schindler, D., Donahue, W., 2006. An impending water crisis in Canada's western prairie

575 provinces. Proc. Natl. Acad. Sci. USA. 103, doi:10.1073/pnas.0601568103.
576 Screen, J., Simmonds, I., 2010. The central role of diminishing sea ice in recent Arctic
577 temperature amplification. Nature 464(29), doi:10.1038/nature09051.
578 Serreze, M., Francis, J., 2006. The Arctic amplification debate. Clim. Change 76(3–4),
579 241–264, doi: 10.1007/s10584-005-9017-y.
580 Serreze, M., Walsh, J., Chapin, E., Osterkamp, T., Dyugerov, P., Romanovsky, M., Oechel,
581 W., Morison, C., Zhang, T., Barry, R., 2000. Observational evidence of recent
582 change in the northern high-latitude environment. Clim. Change 46, 159–207,
583 doi:10.1023/A:1005504031923.
584 Serreze, M., Barrett, A., Stroeve, J., Kindig, D., Holland, M., 2009. The emergence of
585 surface-based Arctic amplification. Cryosphere 3, 11–19, doi:
586 10.5194/tc-3-11-2009.
587 Sewall, J., 2005. Precipitation shifts over western North America as a result of declining
588 Arctic sea ice cover: The coupled system response. Earth Interact. 9, 1–23.
589 Shi, X., Groisman, P., Dery, S., Lettenmaier, D., 2011. The role of surface energy fluxes in
590 pan-Arctic snow cover changes. Environ. Res. Lett. 6, 035204,
591 doi:10.1088/1748-9326/6/3/035204.
592 Storck, P., Lettenmaier, D., Bolton, S., 2002. Measurement of snow interception and
593 canopy effects on snow accumulation and melt in a mountainous maritime climate,
594 Oregon, United States. Water Resour. Res. 38, doi:10.1029/2002WR001281.
595 Stroeve, J. Serreze, M., Barrett, A., Kindig, D., 2011. Attribution of recent changes in autumn
596 cyclone associated precipitation in the Arctic. Tellus A. 63, 1–11.
597 Sturm, M., Racine, C., Tape, K., 2001. Climate change – Increasing shrub abundance in the
598 Arctic. Nature 411, 546–547, doi:10.1038/35079180.
599 Thompson, D., Wallace, J., 1998. The Arctic Oscillation signature in the wintertime
600 geopotential height and temperature fields. Geophys. Res. Lett. 25, 1297–1300.
601 Thompson, D., Wallace, J., 2001. Regional climate impacts of the Northern Hemisphere
602 Annular Mode. Science 293, 85–89.
603 Ye, H., 2001. Increases in snow season length due to earlier first snow and later last snow
604 dates over North Central and Northwest Asia during 1937-94. Geophys. Res. Lett.
605 28(3), 551–554, doi:10.1029/2000GL012036.
606
607 Figure captions

608 Fig. 1. Time series of the Arctic September sea ice extent, the detrended sea ice extent
609 anomalies, and the Arctic Oscillation index in winter (December–February, DJF) during the
610 period of 1979–2006.
611 Fig. 2. Trends of winter (December–February) air temperature (℃/decade) (a) and
612 precipitation (mm/month/decade) (b) during the period of 1979–2006. Regions within
613 contours denote points above the 95% confidence level.
614 Fig. 3. Interannual variability of winter snow depth in Eurasia and North America during the
615 period of 1948–2006.
616 Fig. 4. Monthly variations of decadal averaged snow depth (a, b) and trends of snow depth (c
617 and d), air temperature (e and f), and precipitation (g and h) during two periods (i.e.,
618 1948–2006 and 1979–2006). The left and right panels represent Eurasia and North America,
619 respectively. Asterisks within figures indicate statistical significance at the 95% confidence
620 level.
621 Fig. 5. Linear trends of averaged snow depth in autumn (September–November) (a) and
622 winter (December–February) (b) during the period of 1979–2006. Regions within contours
623 denote points above the 95% confidence level.
624 Fig. 6. The difference between composites for autumn (September–November) following
625 Septembers with actual (top) and detrended (bottom) ice extents that were less than and
626 greater than one standard deviation from the 1979–2006 period mean surface air temperature
627 (a and d), precipitation (b and d), and mean snow depth (c and f), composited for low-ice
628 summers minus high-ice summers.
629 Fig. 7. Linear regressions of averaged surface air temperature (℃/mil. km^2) in winter
630 (December–February) (a and d), precipitation (mm/mil. km^2) (b and e), and mean snow depth
631 (cm/mil. km^2) (c and f) on the detrended September sea ice extent (top) and winter AO index
632 (bottom). Regions within contours denote points above the 95% confidence level.
633 Fig. 8. Linear regression between detrended mean snow depth in autumn
634 (September–November) and soil temperature at 1.2 m depth in the following summer
635 (June–August) during the period of 1979–2006. Regions within contours denote points above
636 the 95% confidence level.

Figure

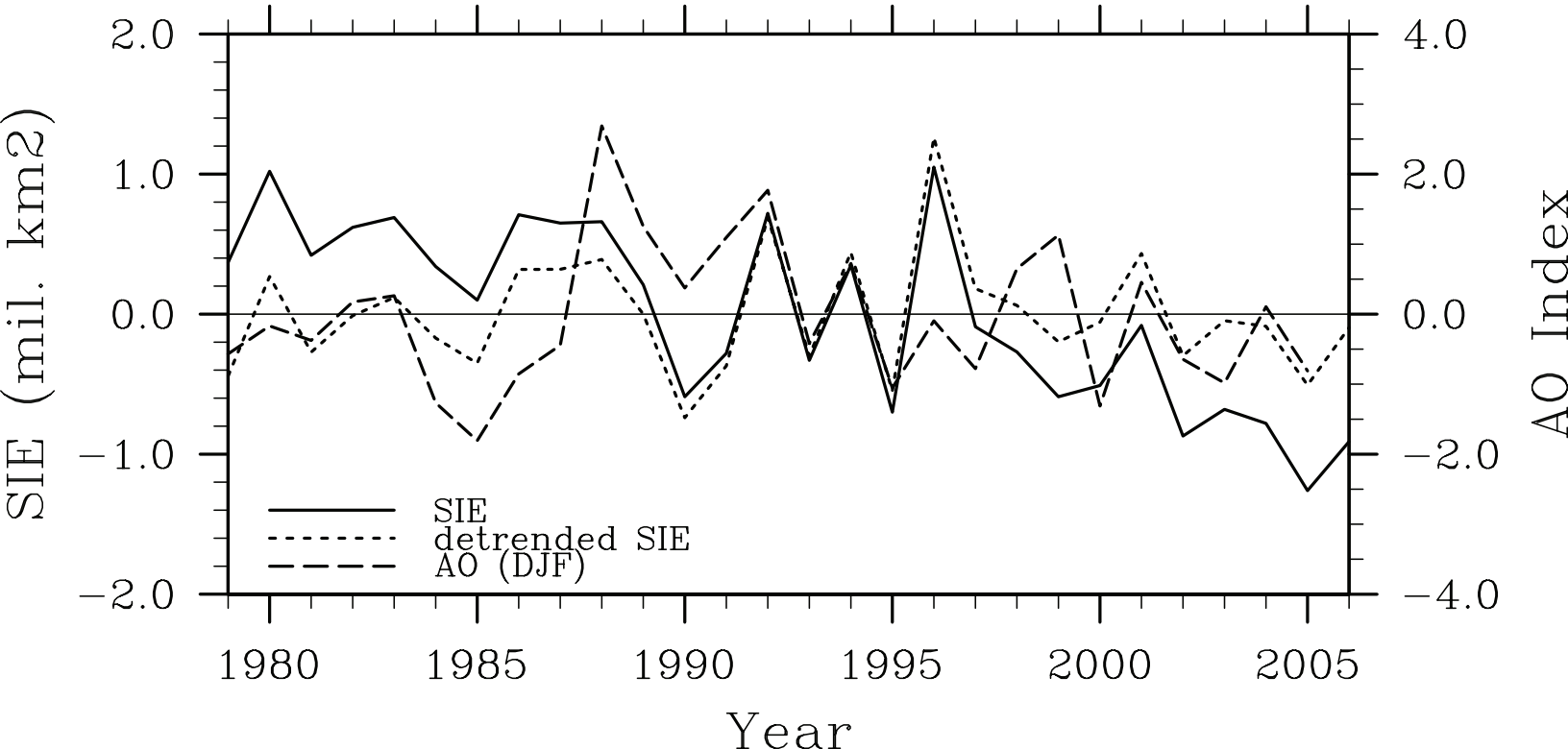
2.0
1.0
0.0
−1.0
−2.0
4.0
2.0
0.0
−2.0
−4.0
SIE (mil. km2)
AO Index
SIE
detrended SIE
AO (DJF)
1980
1985
1990
1995
2000
2005
Year

Figure

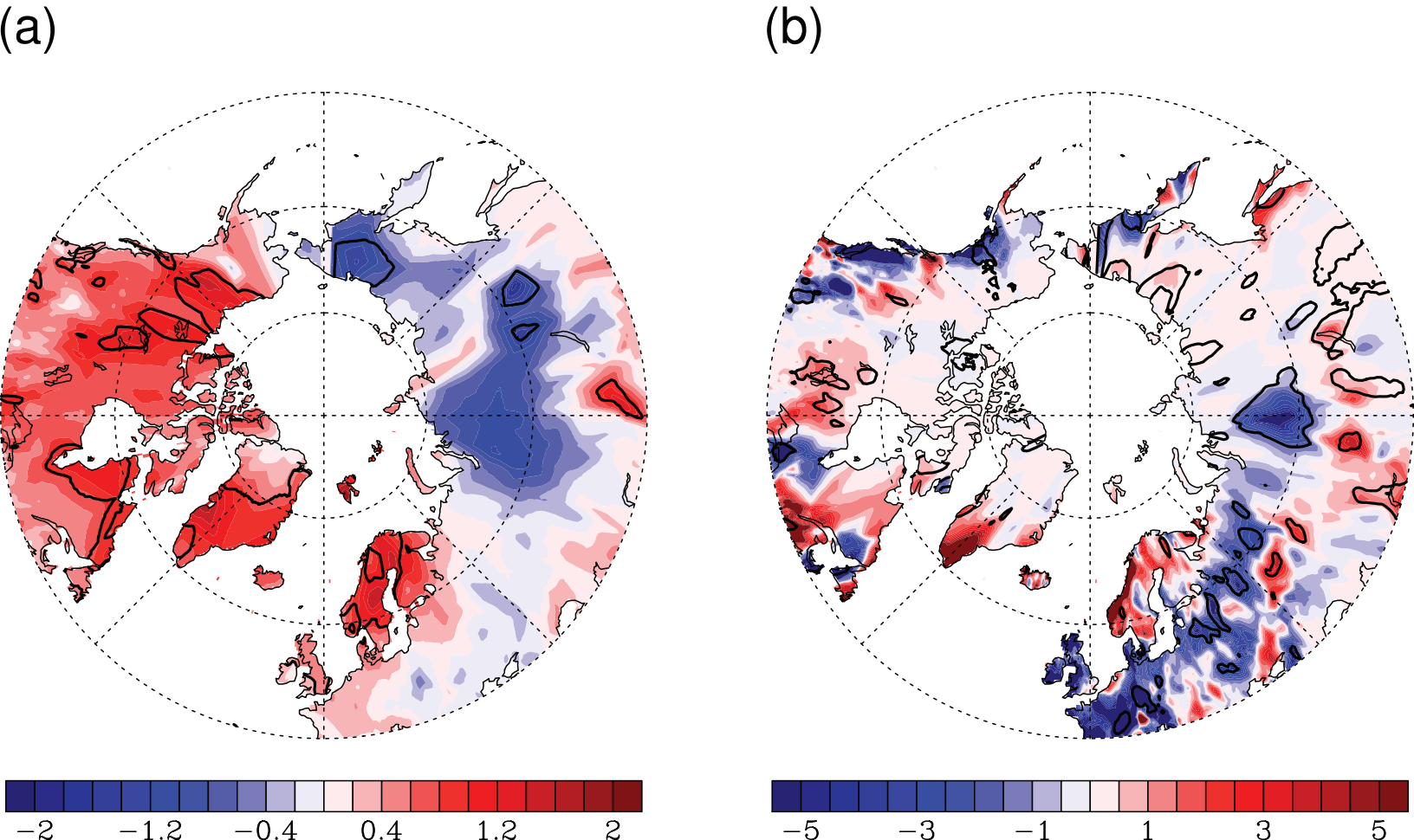

Figure

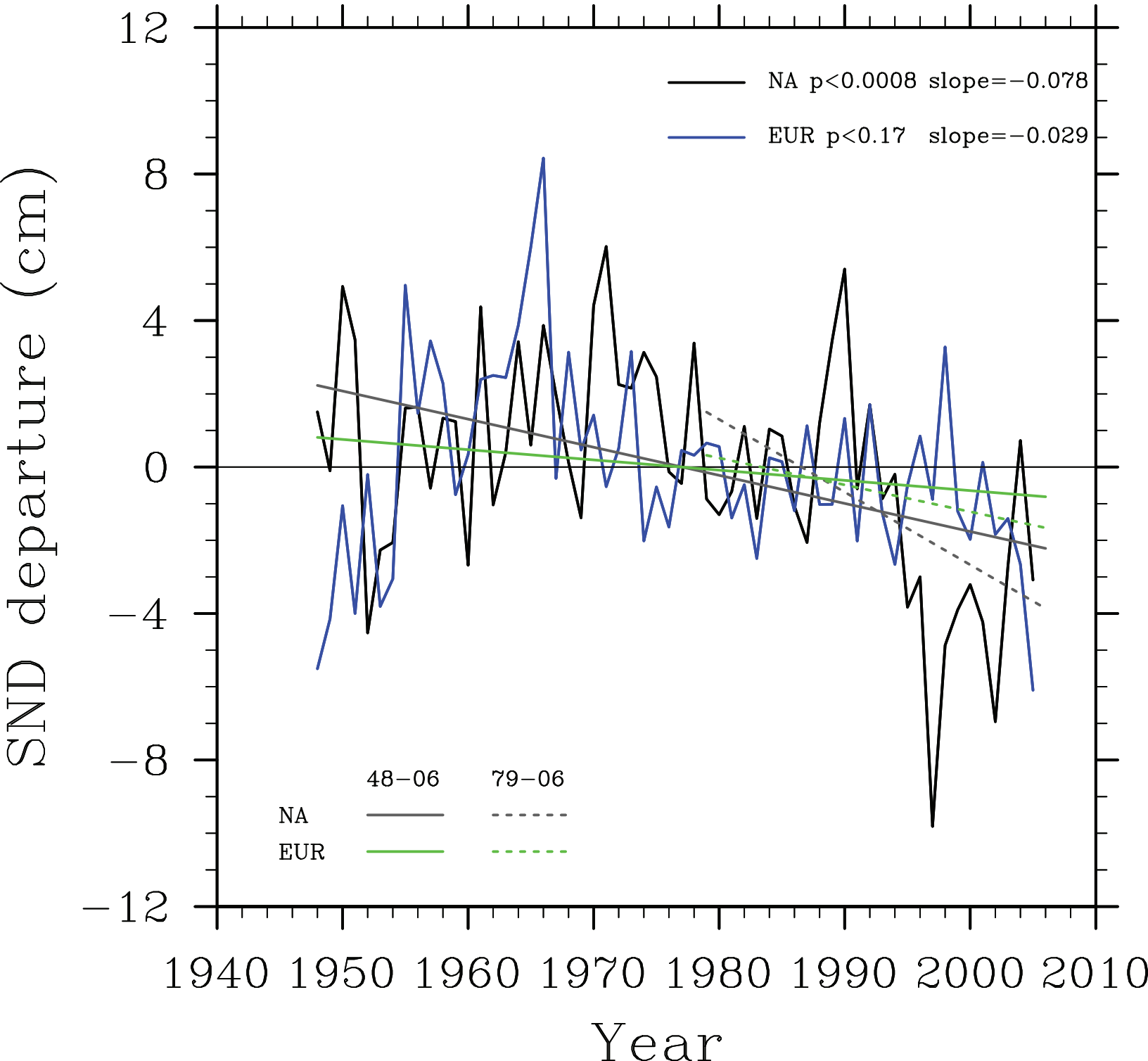
NA p<0.0008 slope=−0.078
EUR p<0.17 slope=−0.029
48−06
79−06
NA
EUR
SND departure (cm)
Year
12
8
4
0
−4
−8
−12
1940
1950
1960
1970
1980
1990
2000
2010

Figure

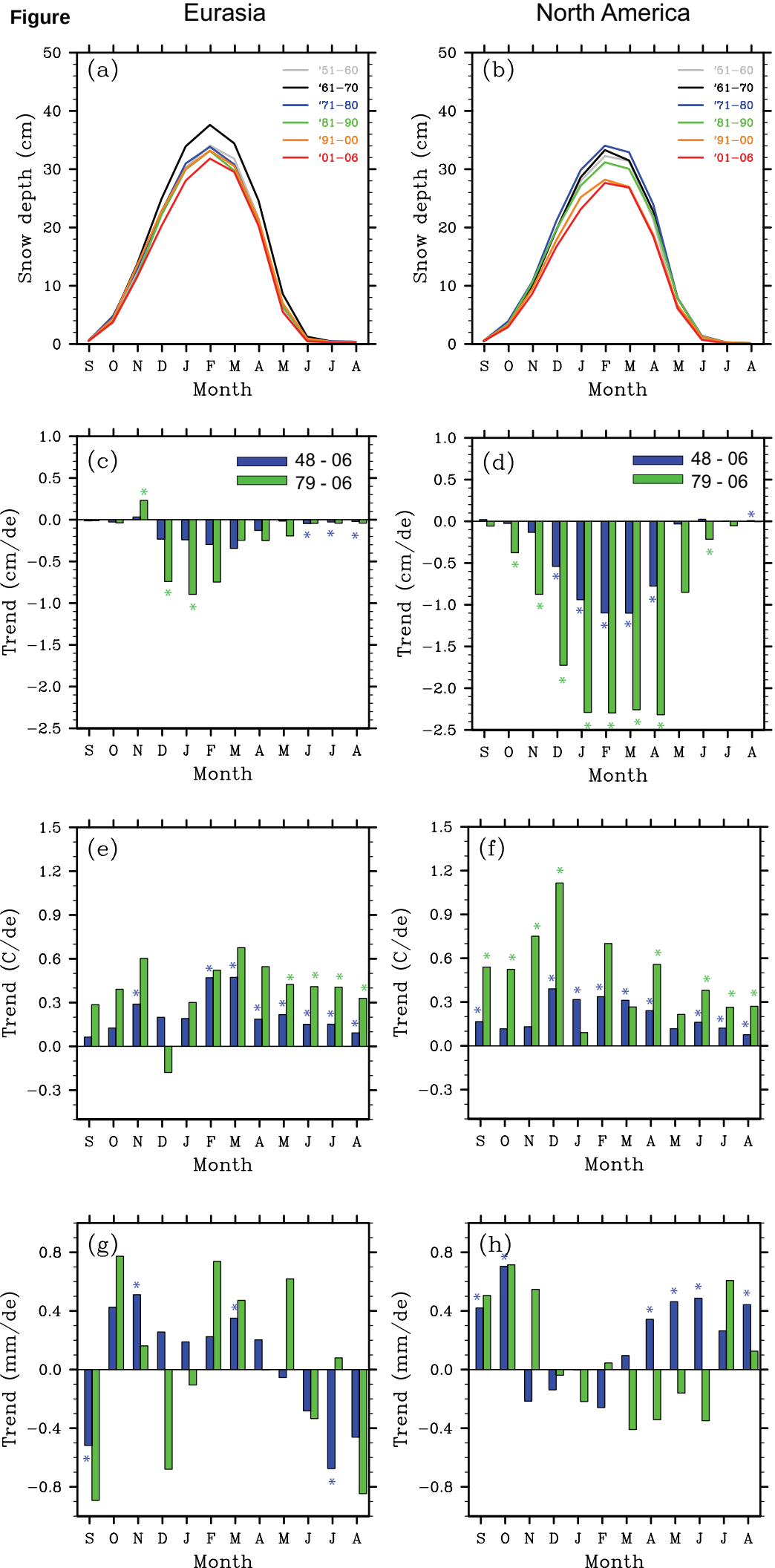
Eurasia
North America
(a)
(b)
(c)
(d)
(e)
(f)
(g)
(h)
'51–60
'61–70
'71–80
'81–90
'91–00
'01–06
48 - 06
79 - 06
Snow depth (cm)
Trend (cm/de)
Trend (C/de)
Trend (mm/de)
Month
S O N D J F M A M J J A

Figure

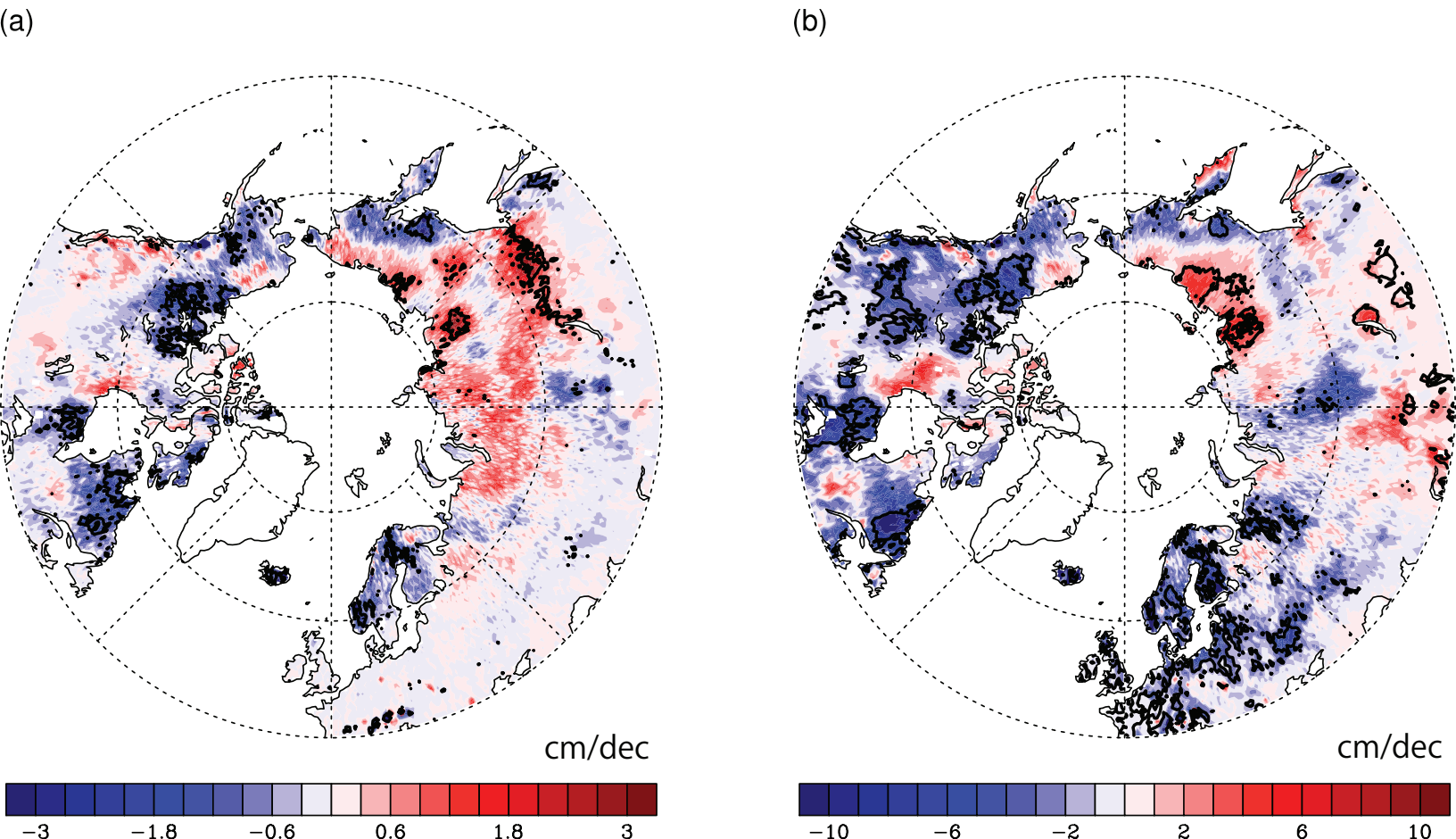

Figure

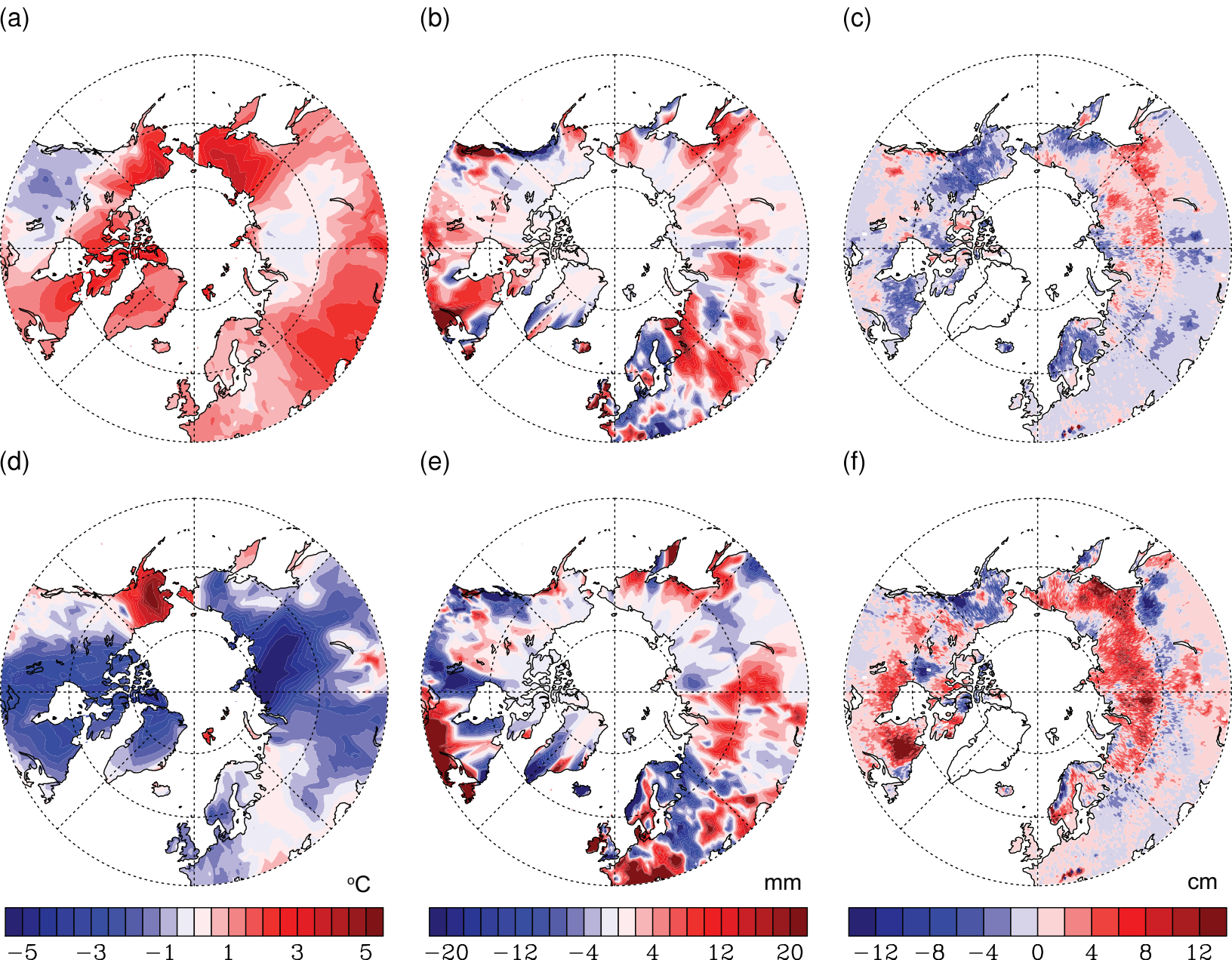

Figure

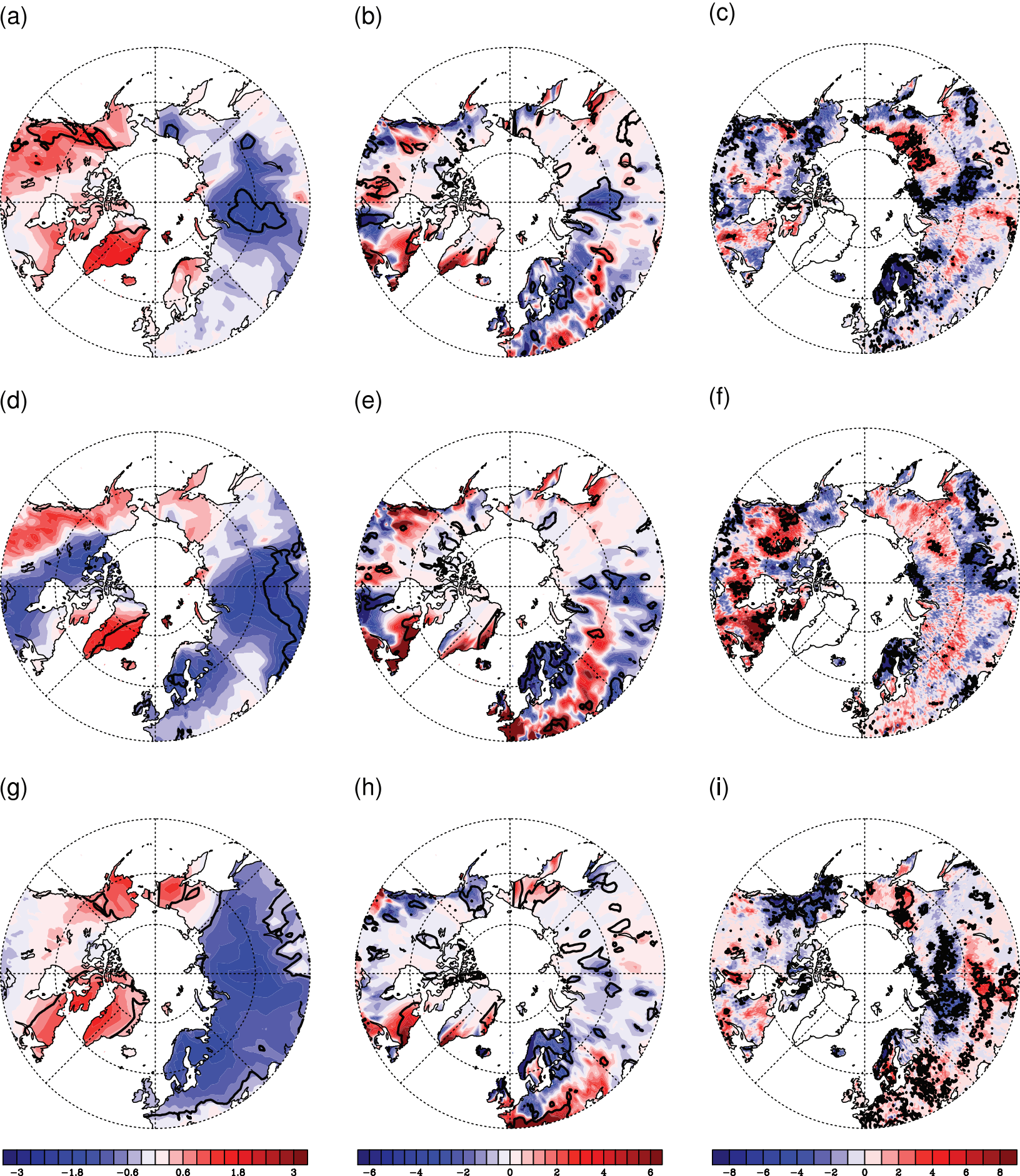

Figure